

SCIENTIFIC REPORTS



OPEN

Symmetry-breaking induced magnetic Fano resonances in densely packed arrays of symmetric nanotrimers

Ning Wang¹, Matthias Zeisberger¹, Uwe Huebner¹, Vincenzo Giannini^{2,3} & Markus A. Schmidt^{1,4,5}

Due to unique properties and great design flexibilities, Fano resonances represent one of the most promising optical features mediated by metallic nanostructures, while the excitation of some Fano modes is impossible due to symmetry reasons. The aim of this work is to show that dense lattice arrangements can have a profound impact on the optical properties of nanostructures and, in particular, can enable the excitation of otherwise dark modes. Here, we demonstrate this concept using the example of rectangular arrays of symmetric trimers packed so densely that the coupling between neighbouring unit cells imposes a symmetry break, enabling the excitation of magnetic Fano resonances. We found that in experiments as well as in simulations, electric and magnetic Fano resonances can be simultaneously formed in cases where the inter-trimer distances are sufficiently small. By analysing the transition from an isolated trimer mode into a regime of strong near-field coupling, we show that by modifying the rectangular unit cell lengths due to the symmetry mismatch between lattice and trimer, two types of Fano resonances can be found, especially magnetic Fano resonances with loop-type magnetic field distributions within the centre of each trimer, which can be either enhanced or suppressed. In addition, the influence of the refractive index environment was measured, showing sensitivity values of approximately 300 nm/RIU. Our work provides fundamental insights into the interaction of the lattice and nanostructure response and paves the way towards the observation of novel optical excitations.

In recent years, nano-optics has attracted substantial attention, with a large number of studies^{1–3} carried out to understand the interaction between light and matter on the nanoscale. By using well-designed plasmonic nanoantennae^{4,5}, sophisticated photonic functionalities have been realized on ultrasmall geometric footprints on the basis of, e.g., deep sub-wavelength metasurfaces^{6,7}, hybrid plasmonic nanosensors⁸, and monolithic fibre nanoprobe⁹.

One particular striking effect mediated by nanostructures is the Fano resonance, which arises from interference between a broadband bright mode and a narrowband dark mode^{10,11}. This modal interaction dramatically changes the lineshape of scattered light by introducing a narrow dip into the extinction spectrum. Due to the low damping of the dark mode, the electromagnetic near-field at the wavelength of the Fano resonance is greatly enhanced, which has the consequence that the scattered light is enhanced accordingly¹². To achieve such a unique effect, numerous types of nanostructures such as single split nanodots^{12,13}, nanocavities¹⁴, nanosphere dimers¹⁵, dolmen-like nanostructures^{14,16}, plasmonic clusters¹⁷ and oligomers^{18–20} are currently being employed. Among these, nanotrimers consisting of three close-packed nanoparticles represent a promising design for realizing the Fano resonance (details of the hybridization are discussed in the Supplementary Information sec. 6). As first experimentally demonstrated in 2010 for the example of self-assembled metal-dielectric spheres²¹, trimers can

¹Leibniz Institute of Photonic Technology, Albert-Einstein-Str. 9, 07745, Jena, Germany. ²The Blackett Laboratory, Department of Physics, Imperial College London, London, SW7 2AZ, UK. ³Instituto de Estructura de la Materia (IEM-CSIC), Consejo Superior de Investigaciones Científicas, Madrid, 28006, Spain. ⁴Abbe School of Photonics and Faculty of Physics, Max-Wien-Platz 1, 07743, Jena, Germany. ⁵Otto Schott Institute of Materials Research, Fraunhoferstr. 6, 07743, Jena, Germany. Correspondence and requests for materials should be addressed to M.A.S. (email: markus-alexander.schmidt@uni-jena.de)

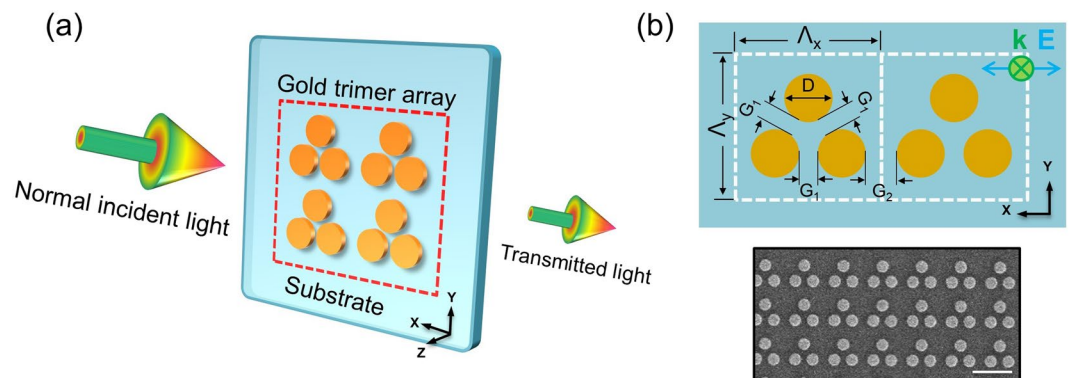


Figure 1. Schematic of the square lattice trimer array incl. the relevant structural parameters. **(a)** Sketch of four trimers located on a silica substrate and excited by polarization-controlled light. Each trimer unit is composed of three symmetrically arranged gold nanodisks. The red frame highlights the dense distribution of the trimer array. **(b)** Details of the symmetric trimer geometry (top) with a corresponding scanning electron micrograph (SEM) image (bottom). The symmetric trimer shares the same inter-dot distances G_1 between all three nanodisks. Here, G_1 and G_2 are named as the intra-trimer gap and inter-trimer gap, respectively. The blue double-headed arrow with the green cross indicates normal incidence and the light polarization along the x-axis. The scale bar in the SEM image refers to $1 \mu\text{m}$.

exhibit a strong magnetic resonance. Later, several studies^{22–25} tried to obtain this magnetic enhancement in trimers by symmetry breaking within the trimer and have successfully shown excitation of magnetic-based Fano resonances with the magnetic resonance being the dark mode. In contrast to an internal symmetry break, the aim of this study is to show that excitation of magnetic Fano resonances in symmetric trimers can be achieved by placing them into densely packed arrays, with the symmetry breaking induced by the lattice arrangement. Here, the trimers are arranged in a rectangular lattice (two-fold symmetry) breaking the three-fold symmetry of the otherwise symmetric trimer unit.

For a majority of the Fano resonances mentioned above, arrays of trimer arrays are used where inter-trimer distances are chosen such to significantly exceed the individual trimer resonance wavelength¹⁶. In a denser configuration, the compact geometrical arrangement leads to strong near-field unit cell interactions, with the diffractive coupling of localized plasmonic resonances^{26,27} further modifying the resonance lineshape. For instance, Chen Yan *et al.*¹⁶ have demonstrated that the optical response of arrays of nanodolmens can be significantly altered by the near-field coupling to adjacent unit cells. By varying the periodicities, the far-field response of the plasmonic system can be evolved into a tight-binding regime or a hybridization regime showing a combined response of the individual trimer response and of the diffraction of the array. However, a detailed investigation for this type of hybrid response between nanostructures and inter-unit cell diffractive coupling has not been intensively carried out to date.

In this report, we reveal the optical properties of densely packed arrays of nanotrimers and their dependence on the geometrical parameters, such as intra-trimer gaps and array pitch. We conducted a set of experiments as well as numerical calculations with a focus on the trimer modes and found that magnetic Fano resonances can be excited for the symmetric trimer geometry when the trimers are arranged in densely packed arrays, with the symmetry breaking induced by the lattice arrangement and not by the individual trimer unit. The report is arranged as follows: First, we analyse the extinction spectrum of the trimer array and find a magnetic Fano resonance mode, identified by its experimental spectral features and simulated near-field distributions^{28,29}. Second, to further explore the impact of the near-field coupling effect on Fano resonances, extinction spectra with varying trimer-to-trimer distances were modelled and analysed. Finally, the trimer arrays were optically characterized under various refractive index (RI) environments. The results indicate that an asymmetric refractive index arrangement between substrate and superstrate weakens the formation of magnetic Fano resonances.

Design and Fabrication

The trimer array is fabricated by lift-off technology using electron beam lithography and dry etching³⁰ (a sketch of one sample is shown in Fig. 1). The fabrication details can be found in the Supplementary Information (SI) in Sec. 3. The array of trimers has a size of $110 \times 110 \mu\text{m}^2$ covering the beam spot of the $20\times$ objectives used in the optical characterization experiments. Each trimer unit is composed of three identical planar gold nanodisks (diameter 425 nm) with a G_1 (intra-trimer gap, sketch in Fig. 1(b)) of 75 nm. The choice of a gold film thickness of 40 nm was mostly based on preliminary fabrication experiments (i.e., this thickness gave the best nanostructures) and has no substantial influence on the mode formation discussed in the remaining part of the manuscript. For the specific sample used in the characterization and RI sensing experiments, the value for G_2 (inter-trimer gap, sketch in Fig. 1(b)) was chosen to be 175 nm, corresponding to an array pitch Λ of 1100 nm. The scanning electron micrograph (SEM) image shown in Fig. 1(b) clearly demonstrates the compactness of the trimer array. Note that in all the extinction data, the polarization of the incident light is along the x-axis.

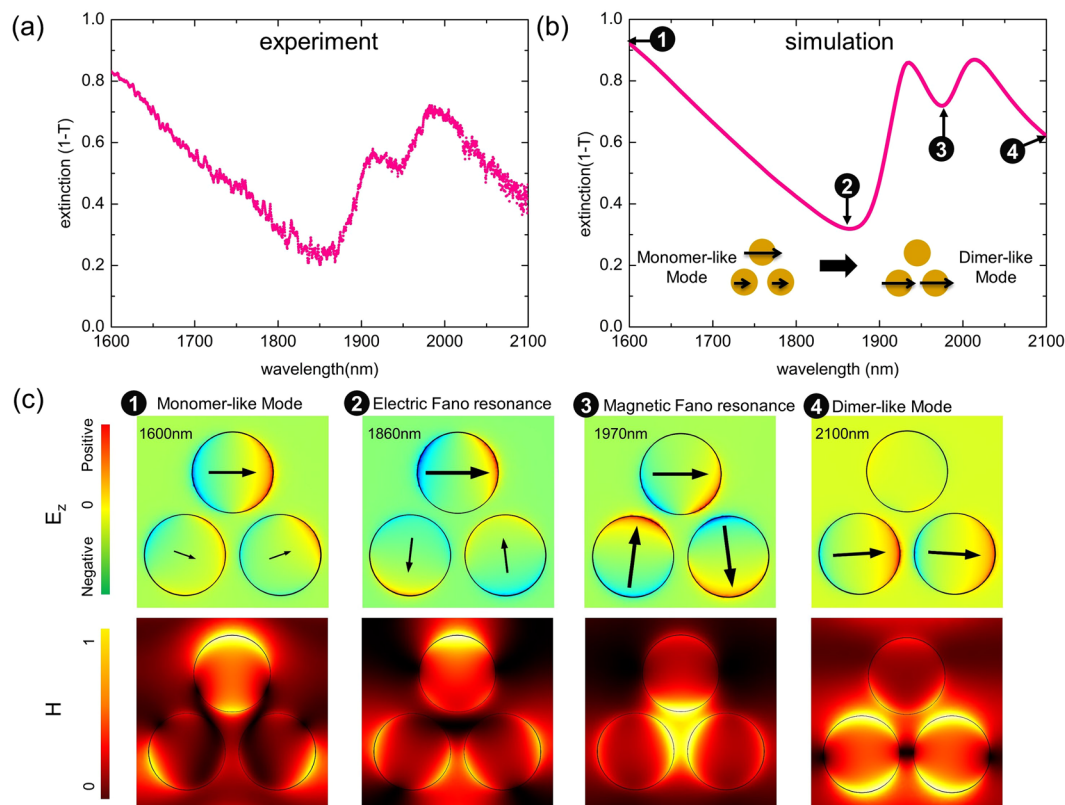


Figure 2. (a) Measured extinction spectrum and (b) corresponding numerical simulation for a trimer array with selected near-field patterns shown in (c) (array pitch Λ : 1100 nm, SEM in Fig. 1(b)). Polarization directions (arrows) and distribution of the out-of-plane electric field component E_z (colour indicates the charge distribution) of one trimer unit cell at a fixed point of time are shown in the upper row of (c) together with the normalized magnetic field distributions in the lower row. The number labels correspond to the wavelengths highlighted in (b). Each image shown in (c) corresponds to an area of $1 \times 1 \mu\text{m}^2$.

Discussions

Magnetic Fano resonance in closely packed trimer arrays. As a first step, we characterize the optical response of the trimer array (D : 425 nm H : 40 nm G_1 : 75 nm) for a fixed pitch (1100 nm, G_2 : 175 nm). In Fig. 2, we show the measured and simulated trimer extinction spectra (from 1600 nm to 2100 nm) together with the simulated near-field patterns at selected spectral positions. Within this specific spectral domain, each individual nanoparticle of one trimer behaves like a dipole, meaning that a more complex (multipolar) response for the individual nanodot does not need to be considered. According to the spectra shown in Figs S1 and S2 (Supplementary Information section 1 and 2), the spectral response of closely packed trimer arrays exhibits a highly asymmetrical lineshape and a strong polarization dependence, which contrasts with the isolated trimers discussed in refs.^{31–34}. Hence, we carried out a set of studies with a focus on these densely packed trimers. In addition, only x-polarized incident light is applied since the polarization influence is beyond the scope of this work.

To obtain a homogeneous RI environment along the vertical direction (Fig. 2(a)), the trimer samples are immersed in a liquid that matches the RI of the substrate ($n = 1.44$). For spectral measurements, a commercial broadband supercontinuum source (NKT Photonics SuperK Compact) was employed for illumination, with the transmitted light recorded by a spectrometer (Instrument Systems SP320-124). Two transmitted spectra were recorded with one beam directed to the respective trimer array and the other passing through an unstructured part of the silica substrate. The experimental transmission T is then obtained by the power ratio of the two spectra. Please note that in this report, we present extinction spectra obtained using $(1 - T)$.

Corresponding numerical calculations (Fig. 2(b)) based on the finite-element-method (FEM) are also conducted in the index-matched configuration by applying periodic boundary conditions. The simulated electric field (E_z , i.e., the component perpendicular to the sample surface - see Fig. 2(c) upper row) plus polarization arrows indicate the charge distributions for the trimer. The electric field data are taken from a plane that is located 1 nm above the disks ($z = 41$ nm), with the polarization distribution calculated within the middle plane ($z = 20$ nm) of the nanodisks. In addition, the spatial distribution of the magnetic field ($|H|$ at $z = 50$ nm) is presented to help one to understand the formed trimer modes in this lattice arrangement. The experimental spectrum coincides well with numerical simulations (Fig. 2(a,b)) where the two main minima are both fully captured (one minimum is near to 1850 nm, and the other minimum is close to 1950 nm) even though the amplitude of the features are slightly different.

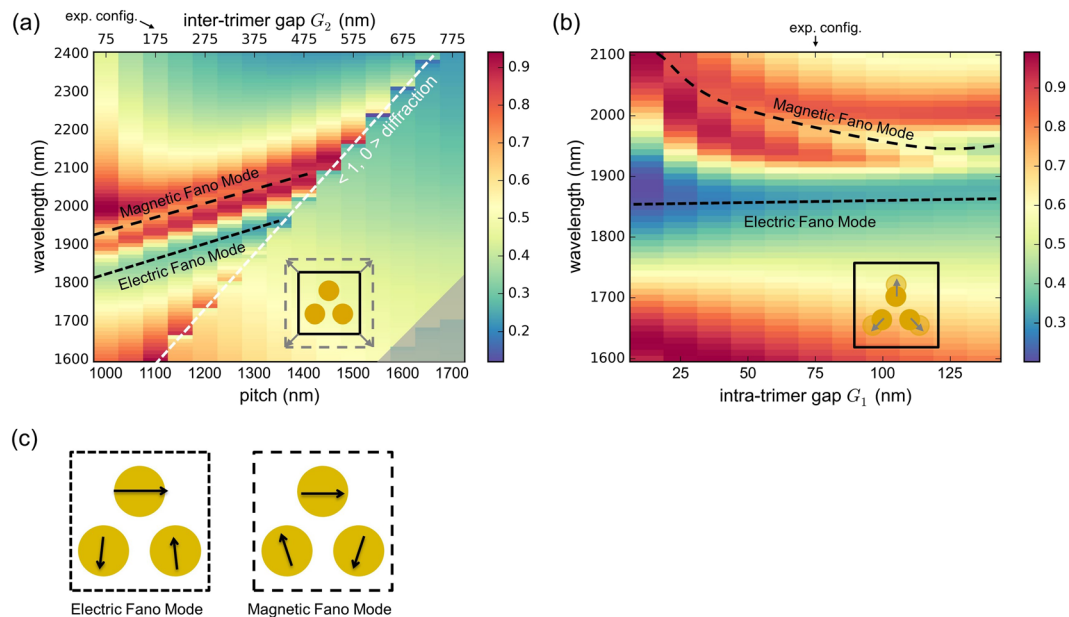


Figure 3. Simulations showing the spectral distribution of the extinction of one trimer in a square unit cell as a function of (a) pitch Λ ($G_1 = 75$ nm) and (b) inter-trimer distance G_1 (pitch is fixed to 1100 nm). The white dashed line in (a) indicates the onset of $\langle 1, 0 \rangle$ diffraction order in the index-matched configuration. The variation of the unit cell is schematically depicted in the lower right corner. The area denoting higher lattice modes is greyed out. The sketch shown in (b) displays the extinction in case the intra-trimer gaps are modified. (c) Schematics of the distribution of the trimer nanodot dipole moments relevant within the scope of this work. The evolutions of these two patterns in (a) and (b) are indicated by the appropriate dashed lines. The configurations targeted in the experiments presented here are indicated at the top of (a) and (b).

At the sides of the investigated spectral domain (points 1 and 4 in Fig. 2(b)), the related field patterns (Fig. 2(c)) exhibit dipolar excitations of the upper particle (monomer excitation) and the two lower particles (dimer excitation), showing a transition from a monomer-like mode to a dimer-like mode (schematically illustrated in Fig. 2(b)). Between these two cases, two extinction minima (points 2 and 3 in Fig. 2) are found corresponding to different Fano resonance modes. At a wavelength of 1860 nm (point 2), a dipolar excitation of the upper and quadrupolar excitations of the two lower dots are observed, resembling a dolmen-like electric Fano pattern^{14,16}.

It is of great interest to note the loop-like polarization distribution (named as magnetic Fano resonance in Fig. 2(b,c)) situated at the extinction dip close to 1970 nm. In particular, the magnetic field (case 3 in Fig. 2(c)) at this wavelength is highly confined within the inner area of the trimer unit, which cannot be found at any of the other three wavelengths. This pattern has been intensively discussed in the literature and has been identified as a magnetic-based coil-type Fano resonance^{23–25}. Here, the bright mode, formed by the three individual dipole modes being in electric resonance, couples to the magnetic resonance resulting in the circle-like polarization distribution. Therefore, destructive interference of the bright electric mode and the dark magnetic mode results in an extinction dip as confirmed in simulations and experiments. Several reports reveal that this magnetic Fano resonance requires additional symmetry breaking (modifying inter-particle gaps²² or geometry of trimer dots²³, etc.) to be excited. This mode is assumed to be forbidden for an individual isolated symmetric trimer or for a sparse array of trimers^{31,32} since its total electric dipole moment is zero. In addition, its magnetic dipole moment is perpendicular to the sample surface. Therefore, this mode cannot be excited by a plane wave at normal incidence. However, in this closely packed trimer array where the coupling to neighbouring unit cells cannot be neglected, we experimentally observe spectral features for the magnetic Fano resonance modes. In the following sections, we will explore how the coupling between different trimer units can influence the overall optical response of the investigated arrays.

Trimer plasmon modes in a square-shaped unit cell. The following section discusses the impact of the intra-trimer gap (G_1) and inter-trimer gap (G_2) on the spectral behaviour with the trimer located in the centre of a square-shaped unit cell. Here, the diameter (D) and height (H) of the dots is fixed to 425 nm and 40 nm, respectively. For convenience, we address our study to the periodic constant (pitch) Λ instead of the inter-trimer gap G_2 ($\Lambda = 2 \times D + G_1 + G_2$). In detail, the spectral distribution of the extinction for various values of pitches (1000 nm $< \Lambda < 1700$ nm; steps of 50 nm; G_2 : 75 nm to 775 nm; G_1 is fixed at 75 nm) is presented in Fig. 3(a). Additionally, Fig. 3(b) shows the simulated extinction spectra obtained by modifying the intra-trimer gap G_1 from 12.5 to 132.5 nm in steps of 12.5 nm. Both calculations are carried out in the index-matched configuration (incident polarization is along the x-polarized direction) with the white dashed line (Fig. 3(a)) indicating the $\langle 1, 0 \rangle$ diffraction order in this configuration.

Overall, the extinction spectra can be dramatically modified by varying the inter- and intra-trimer gaps. In Fig. 3(a), electric and magnetic Fano resonance are observed at pitch values between 1000 and 1400 nm, which are indicated by short-dashed and long-dashed black lines. Within this range of pitches, the trimer-to-trimer

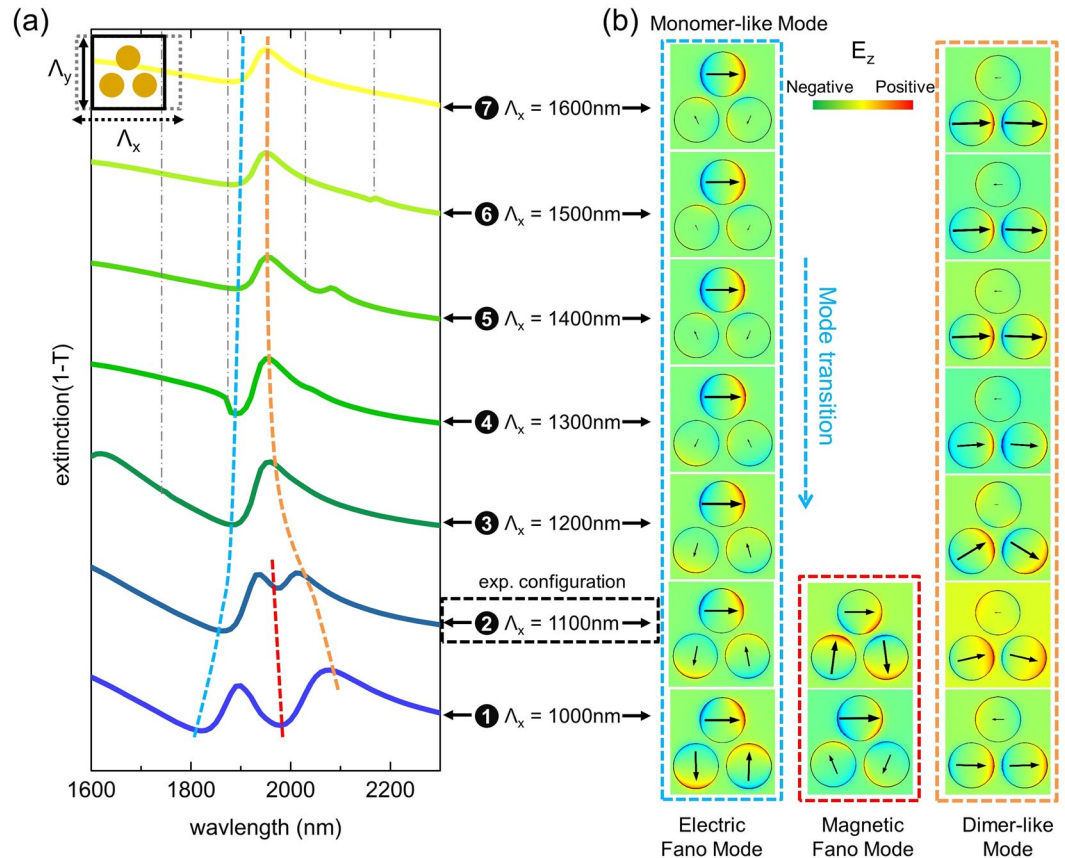


Figure 4. (a) Dependence of the spectral distribution of the extinction of the rectangular lattice trimer array for the case when the pitch is changed along the horizontal direction (x -axis) while no change is assumed along the vertical direction. The schematic in the top-left corner illustrates how the unit cell is modified. The vertical pitch is set to $\Lambda_y = 1100$ nm and Λ_x varies from 1000 to 1600 nm. (b) Corresponding simulated electric field patterns and polarization distributions at a fixed point in time at the wavelengths highlighted by the various dashed lines in (a). The designated number together with horizontal pitch Λ_x connects the spectral features and near-field patterns. Note, in the blue dashed frame, the transition of the mode from a monomer-like pattern to an electric Fano resonance pattern is clearly visible. The dashed coloured lines are guides-to-the-eye to highlight the spectral shift of the respective feature. The vertical dash-dot grey lines indicate the onsets of the $\langle 1, 0 \rangle$ diffraction orders. The experimental configuration measured is also highlighted by the box framed by the black dashed line.

coupling distance G_2 is gradually varied while the dot-to-dot interaction remains the same (G_1 is fixed). Noticeably, both patterns shift towards longer wavelengths, which indicates that the modal interactions can be modified by the lattice-induced coupling. Once the pitch exceeds 1400 nm, the extinctions only exhibit step-like lineshapes along the onset of the first diffraction order ($\lambda = n \times \Lambda$) in the medium ($n = 1.44$), whereas the distributions referring to electric and magnetic Fano resonance can no longer be observed. More sophisticated lattice modes in the left corner are greyed out since they are beyond of this article.

Now we consider a complex coupling configuration where the intra-trimer gap G_1 and inter-trimer gap G_2 are both modified. Figure 3(b) displays simulated extinction spectra that are obtained by varying the intra-trimer gaps G_1 (from 75 nm to 137.5 nm) for a fixed pitch ($\Lambda = 1100$ nm). In this case, the gap size G_2 is correspondingly changed from 237.5 to 112.5 nm. Surprisingly, the central spectral position of electric Fano resonance remains at approximately 1850 nm, while magnetic Fano resonance reduces in wavelength from approximately 2100 to 1970 nm. This blue-shift of the magnetic Fano resonance with increasing gap separation agrees well with the discussion in ref.²¹

We need to point out that the emergence of the magnetic Fano resonance mode strongly relies on the near-field coupling of neighbouring unit cells. In Fig. 3(a), the spectral feature of the Fano resonance is most evident at a pitch of 1000 nm, where the inter-trimer gap distance reaches the minimum value investigated here ($G_2 = 75$ nm, G_1 is 75 nm). This amplitude enhancement for the Fano resonance mode is also visible in Fig. 3(b) when decreasing G_2 . In particular, at the minimum value of G_2 (Fig. 3(b)), the array cannot be divided into individual trimer unit cells since the inter-trimer coupling of the lower two dots is stronger than the intra-trimer interactions, i.e., G_2 is smaller than G_1 (G_2 112.5 nm and G_1 137.5 nm).

Trimer behaviour for the case when the coupling is varied along the horizontal or vertical coupling direction. In this section, we study the impact of the inter-unit cell coupling on the overall extinction spectra by altering the unit cell along the horizontal (x -axis) and vertical (y -axis) directions. For the following

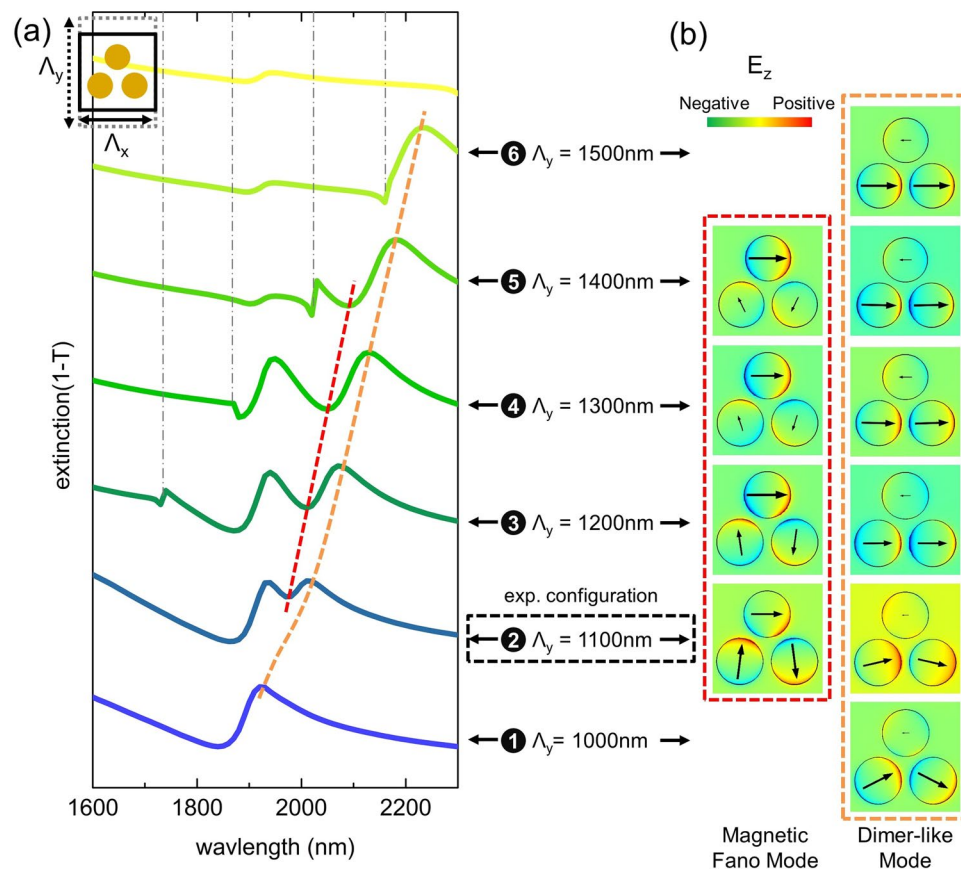


Figure 5. (a) Dependence of the spectral distribution of the extinction in case the pitch is changed along the vertical direction (y-axis, schematic in the top-left corner). Λ_y varies from 1000 to 1500 nm, while the horizontal pitch Λ_x is set to 1100 nm. (b) Corresponding simulated electric field patterns and polarization distribution at the wavelengths highlighted by the various dashed lines in (a). The designated number together with the horizontal pitch Λ_y connects spectral features and near-field patterns. The dashed coloured lines are guides-to-the-eye showing the spectral shift of the respective feature. The vertical dash-dot grey lines indicate the $\langle 0, 1 \rangle$ diffraction order. The experimentally investigated configuration is highlighted by the framed box.

numerical simulations, arrays of trimers with a dot diameter of $D = 425$ nm, height of $H = 40$ nm and intra-trimer gap of $G_1 = 75$ nm are numerically investigated assuming a homogenous RI environment. Using a periodic boundary condition, the corresponding simulation results are presented in Figs 4 and 5. Here, the horizontal and vertical edges of the rectangular unit cell are named in the following as Λ_x and Λ_y , respectively.

We first examine the trimer spectra and mode profiles by merely extending Λ_x from 1000 to 1600 nm (G_2 : 75 to 675 nm) while keeping the vertical pitch constant ($\Lambda_y = 1100$ nm). The simulations are presented in Fig. 4 with a sketch used to show how the unit cell is modified (left upper corner in Fig. 4(a)). Two distinct modes dominate the overall extinction response, namely, the monomer-like mode (extinction minima, blue-dashed line) and the dimer-like mode (extinction maxima, orange-dashed line), which both roughly remain at the same spectral position when $\Lambda_x > 1200$ nm (monomer mode: at approximately 1900 nm; dimer mode: close to 1950 nm). For such large horizontal pitches, the inter-trimer gaps G_2 are larger than 275 nm, being nearly four times the size of the intra-trimer gap G_1 (75 nm), with the result that the inter-trimer coupling is smaller than the inter-dot coupling. Hence, the trimers behave like individual elements and the interplay between the monomer mode and dimer mode is less pronounced.

As highlighted by the blue dashed line in Fig. 4(a), a transition from a monomer-like mode (cases 7 to 3) to an electric Fano mode (case 2 and 1) is clearly observable. In particular, for $\Lambda_x = 1000$ nm, the inter-trimer coupling along the x-axis is maximal, with both electric and magnetic Fano modes clearly visible in the corresponding spectrum. Here, the magnetic Fano resonance mode becomes most prominent, i.e., the respective extinction minimum is most distinct among all the spectra presented.

The next step in the analysis targets the understanding of the impact of the vertical coupling on the optical response. Here, the extinction spectra for the trimer arrays in a rectangle cell with variation along the y-direction are calculated (G_1 and G_2 are fixed to 75 nm and 175 nm, respectively, with $\Lambda_x = 1100$ nm). Through varying Λ_y , we obtain a set of extinction spectra that are shown in Fig. 5(a), which are accompanied by corresponding near-field distributions (Fig. 5(b)). Here, the trimer response becomes more complicated and highly asymmetric due to enhanced coupling between the trimers at the onset of the first diffraction order. Nevertheless, a dimer-like pattern (orange dashed line) can be observed for all six cases, while the corresponding extinction maximum shifts

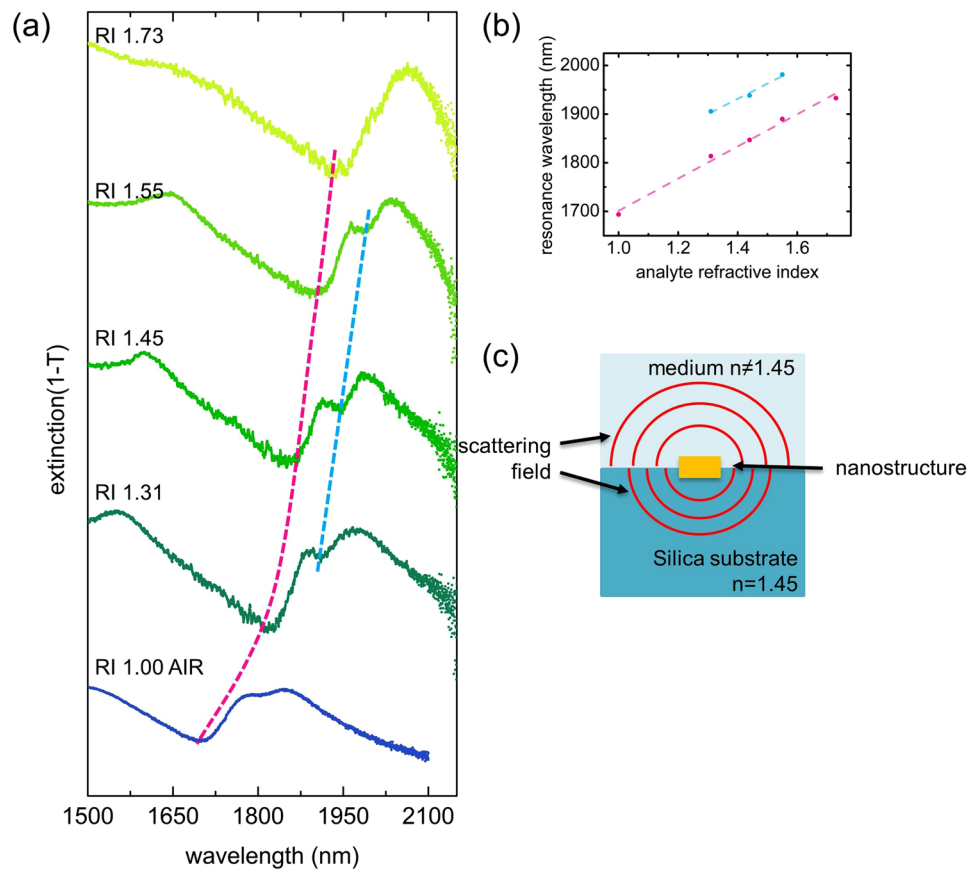


Figure 6. (a) Measured extinction spectra for the trimer array for different vertical RI configurations (the superstrate refractive index was changed by immersing the sample into different liquids). The dashed magenta and blue curves are guides-to-the-eye and indicate the spectral redshift of the electric and magnetic Fano resonances (shown in Fig. 2), respectively. (b) Resonance wavelength (left axis) as a function of superstrate RIs. The dashed lines are linear fits to the data points. (c) Illustration showing the different scattering fields in the situation of an inhomogeneous refractive index environment.

towards longer wavelengths when increasing Λ_y . For cases 2 to 5 (pitch increases from 1100 to 1500 nm), the magnetic Fano resonance is formed, which is evidenced by the respective extinction minimum (red dashed curve in Fig. 5(a)). Inspection of the corresponding near field patterns (red frame) shows that for the case when Λ_y is increased, the amplitude of the excitation of the lower two dots is reduced while the top dot shows a gradually stronger response. Once $\Lambda_y > 1500$ nm, the magnetic Fano resonance cannot be observed anymore.

At this stage, we would like to conclude the discussion of the impact of the near-field coupling on the formation of the magnetic Fano resonance obtained from the simulated results presented in Figs 3, 4 and 5. First, the spatial distribution of the trimers within the array matters. We clearly observe that in the experiments and in simulations, a magnetic Fano resonance mode is formed in densely packed arrays of symmetrical trimers, which should be forbidden for an isolated symmetric trimer based on group theory^{22,32,34}. Here, we attribute the formation of the magnetic Fano resonance to the symmetry breaking imposed by the square lattice, i.e., to the fact that the trimers and the array have different symmetries. Specifically, the square-shaped lattice breaks the three-fold symmetry of individual trimers, enabling the magnetic and electric modes of the trimer to interact. Second, symmetry breaking-mediated formation of the magnetic Fano resonance only works under particular conditions, i.e., only for certain combinations of lattice parameters, wavelength and incident light polarization. For instance, according to the square-shaped unit cell studied in Fig. 3(a), the pitch should not exceed 1400 nm to trigger the formation of the magnetic Fano resonance. For this configuration, the impact of diffraction can be suppressed below the actual operation wavelength while the inter-unit cell coupling remains effective. Finally, we would like to emphasize again that the trimer-to-trimer coupling plays a more important role for the formation of the magnetic Fano resonance compared to the dot-to-dot interaction within a trimer unit. This phenomenon can be found in Figs 3(b) and 4(a), where a complete loop-like polarization is gradually formed when decreasing the inter-trimer gap G_2 .

Trimer plasmon modes in various RI environment. Detecting small changes of the refractive index in nanoscale environments is of key importance for numerous fields particularly within the fields of bioanalytics and molecular sensing, representing a topic that is intensively addressed by the nanophotonics community^{35–39}. To understand the impact of the RI environment on the optical response of the trimer array and to determine the related RI sensitivity, we immersed the samples into different RI liquids ($n = 1.31$

to 1.73) and measured the extinction under normal incidence (Fig. 6). In general, the resonance dip, being located near 1650 nm (electric Fano resonance in Fig. 2) in the situation of an air superstrate, shifts towards longer wavelengths as the RI of the liquids increases (this spectral red-shift is highlighted in Fig. 6(a) by the dashed magenta line). The magnetic Fano resonance mode is only found in three of the five extinction spectra ($n = 1.31, 1.44$ and 1.55). The corresponding wavelengths for the resonances are plotted in Fig. 6(b) and are fitted by linear functions to obtain the RI sensitivity. This procedure yields an RI sensitivity of 312.8 nm/RIU (coefficient of determination $R^2 = 96.9\%$) for the electric Fano-like mode and 330.5 nm/RIU (coefficient of determination $R^2 = 98.8\%$) for the magnetic Fano resonance mode. Compared to sensitivities obtained in other types of plasmonic structures (nanodisks (~ 180 nm/RIU in VIS⁴⁰), lattices of trimers (~ 170 nm/RIU in VIS⁴¹, ~ 370 nm/RIU in IR⁴¹)), our densely packed trimer arrays offer sensitivities of the same order, which are comparable to other Fano resonance sensors (approximately 300 nm/RIU in nanohole quadrupers⁴² and heptamer cluster⁴³). One advantage of our structure is that the area covered by the array can be minimized to several μm^2 due to the dense configuration. As reported in ref.⁴⁴, we designed a trimer-based fibre sensor, where the diameter of the sensing area is approximately $100 \mu\text{m}^2$ enabling one to perform sensing with the light from the fibre core only, which would otherwise be difficult if the array was very sparse.

It is important to note that the magnetic Fano resonance mode is more pronounced for the case when the particle array is immersed in the liquid with an RI equal to that of the substrate. In this case, a unique relationship between the scattered field and the pitch is obtained because the wavenumber of the scattered wave is the same as that in the substrate and in the superstrate. For the RI-mismatched situation (the bottom and top case in Fig. 6(a)), the two different RIs impose two scattered waves at the same vacuum wavelength (schematically illustrated in Fig. 6(c)). Hence, the distribution of the scattered energy into two waves with different wavenumbers leads to weaker spectral features rather than the strong feature realized in the case of a homogeneous environment.

Conclusion

Artificial nanostructures have appreciably promoted the development of nanophotonics research in the last decade, with a multitude of novel optical effects discovered with one of the most important examples being the Fano resonance. In this report, we have studied the impact of the lattice geometry on the optical response of nanotrimers arranged in densely packed square arrays at infrared wavelengths. We found that in experiments as well as in simulations, electric and magnetic Fano resonance modes can be formed in cases when the inter-trimer distances are sufficiently small, i.e., arise solely due to the array arrangement. In particular, the observation that magnetic Fano resonances can be excited in a system that consists of a symmetric nanostructure unit supporting a magnetic Fano resonance as a dark mode only clearly shows that the lattice arrangement imposes a symmetry breaking, making the magnetic Fano resonance visible in the spectral response of the array. By varying the array parameters, we clearly reveal a transition from an isolated trimer mode into a regime of strong near-field coupling, showing magnetic Fano resonances with loop-type magnetic field distributions. This otherwise hard-to-observe excitation only emerges due to the presence of the neighbouring trimer units and the symmetry mismatch between the square lattice and three-fold symmetry of the nanotrimers. Finally, we reveal the impact of different refractive index environments on the optical response of the trimer arrays, with the sensitivity measured to be approximately 300 nm/RIU.

By transferring the concept of lattice-induced symmetry breaking to other nanostructures, our findings provide a pathway towards observing novel kinds of optical excitations and yield a new degree of freedom to design artificial nanocomponents and -devices. Promising applications for the trimer lattice can be envisioned within fields such as nonlinear optics to generate frequencies at desired wavelengths or bioanalytics via high precision sensing⁴⁴. Both examples exploit the unique features of the strongly enhanced electric and magnetic fields generated within the centre of the structure.

References

- Novotny, L. & Hecht, B. *Principles of nano-optics* (Cambridge University Press, 2012).
- Maier, S. A. *Plasmonics: fundamentals and applications* (Springer Science & Business Media, 2007).
- Lal, S., Link, S. & Halas, N. J. Nano-optics from sensing to waveguiding. *Nature Photonics* **1**, 641 (2007).
- Giannini, V., Fernández-Domínguez, A. I., Heck, S. C. & Maier, S. A. Plasmonic nanoantennas: fundamentals and their use in controlling the radiative properties of nanoemitters. *Chemical Reviews* **111**, 3888–3912 (2011).
- Meinzer, N., Barnes, W. L. & Hooper, I. R. Plasmonic meta-atoms and metasurfaces. *Nature Photonics* **8**, 889 (2014).
- Yu, N. *et al.* Light propagation with phase discontinuities: generalized laws of reflection and refraction. *Science* **334**, 333–337 (2011).
- Zeisberger, M., Schneidewind, H., Huebner, U., Popp, J. & Schmidt, M. A. Nanoboomerang-based inverse metasurfaces—a promising path towards ultrathin photonic devices for transmission operation. *APL Photonics* **2**, 036102 (2017).
- Schmidt, M. A., Lei, D. Y., Wondraczek, L., Nazabal, V. & Maier, S. A. Hybrid nanoparticle–microcavity-based plasmonic nanosensors with improved detection resolution and extended remote-sensing ability. *Nature Communications* **3**, 1108 (2012).
- Tuniz, A., Chemnitz, M., Dellith, J., Weidlich, S. & Schmidt, M. A. Hybrid-mode-assisted long-distance excitation of short-range surface plasmons in a nanotip-enhanced step-index fiber. *Nano Letters* **17**, 631–637 (2017).
- Gallinet, B. & Martin, O. J. Influence of electromagnetic interactions on the line shape of plasmonic Fano resonances. *ACS Nano* **5**, 8999–9008 (2011).
- Luk'yanchuk, B. *et al.* The Fano resonance in plasmonic nanostructures and metamaterials. *Nature Materials* **9**, 707 (2010).
- Fang, Z. *et al.* Removing a wedge from a metallic nanodisk reveals a Fano resonance. *Nano Letters* **11**, 4475–4479 (2011).
- Zhang, S. *et al.* Pronounced Fano resonance in single gold split nanodisks with 15 nm split gaps for intensive second harmonic generation. *ACS Nano* **10**, 11105–11114 (2016).
- Verellen, N. *et al.* Fano resonances in individual coherent plasmonic nanocavities. *Nano Letters* **9**, 1663–1667 (2009).
- Yan, J. *et al.* Directional Fano resonance in a silicon nanosphere dimer. *ACS Nano* **9**, 2968–2980 (2015).
- Yan, C. & Martin, O. J. Periodicity-induced symmetry breaking in a Fano lattice: hybridization and tight-binding regimes. *ACS Nano* **8**, 11860–11868 (2014).
- Fan, J. A. *et al.* Fano-like interference in self-assembled plasmonic quadrupole clusters. *Nano Letters* **10**, 4680–4685 (2010).
- Hentschel, M. *et al.* Transition from isolated to collective modes in plasmonic oligomers. *Nano Letters* **10**, 2721–2726 (2010).

19. Hentschel, M., Dregely, D., Vogelgesang, R., Giessen, H. & Liu, N. Plasmonic oligomers: the role of individual particles in collective behavior. *ACS Nano* **5**, 2042–2050 (2011).
20. Miroschnichenko, A. E. & Kivshar, Y. S. Fano resonances in all-dielectric oligomers. *Nano Letters* **12**, 6459–6463 (2012).
21. Fan, J. A. *et al.* Self-assembled plasmonic nanoparticle clusters. *Science* **328**, 1135–1138 (2010).
22. Sheikholeslami, S. N., García-Etxarri, A. & Dionne, J. A. Controlling the interplay of electric and magnetic modes via fano-like plasmon resonances. *Nano Letters* **11**, 3927–3934 (2011).
23. Nazir, A. *et al.* Fano coil-type resonance for magnetic hot-spot generation. *Nano Letters* **14**, 3166–3171 (2014).
24. Panaro, S. *et al.* Plasmonic moon: a fano-like approach for squeezing the magnetic field in the infrared. *Nano Letters* **15**, 6128–6134 (2015).
25. Yang, D.-J. *et al.* Magnetic fano resonance-induced second-harmonic generation enhancement in plasmonic metamolecule rings. *Nanoscale* **9**, 6068–6075 (2017).
26. Auguie, B. & Barnes, W. L. Collective resonances in gold nanoparticle arrays. *Physical Review Letters* **101**, 143902 (2008).
27. Rodriguez, S. R. K. *et al.* Coupling bright and dark plasmonic lattice resonances. *Physical Review X* **1**, 021019 (2011).
28. Nikitin, A. G., Kabashin, A. V. & Dallaporta, H. Plasmonic resonances in diffractive arrays of gold nanoantennas: near and far field effects. *Optics Express* **20**, 27941–27952 (2012).
29. Huang, Y., Ma, L., Hou, M. & Zhang, Z. Universal near-field interference patterns of fano resonances in two-dimensional plasmonic crystals. *Plasmonics* **11**, 1377–1383 (2016).
30. Huebner, U. *et al.* Multi-stencil character projection e-beam lithography: a fast and flexible way for high quality optical metamaterials. In *30th European Mask and Lithography Conference*, vol. 9231, 92310E (International Society for Optics and Photonics, 2014).
31. Alegret, J. *et al.* Plasmonic properties of silver trimers with trigonal symmetry fabricated by electron-beam lithography. *The Journal of Physical Chemistry C* **112**, 14313–14317 (2008).
32. Chuntunov, L. & Haran, G. Trimeric plasmonic molecules: the role of symmetry. *Nano Letters* **11**, 2440–2445 (2011).
33. Chuntunov, L. & Haran, G. Effect of symmetry breaking on the mode structure of trimeric plasmonic molecules. *The Journal of Physical Chemistry C* **115**, 19488–19495 (2011).
34. Brandl, D. W., Mirin, N. A. & Nordlander, P. Plasmon modes of nanosphere trimers and quadrimers. *The Journal of Physical Chemistry B* **110**, 12302–12310 (2006).
35. Sreekanth, K. V. *et al.* Extreme sensitivity biosensing platform based on hyperbolic metamaterials. *Nature Materials* **15**, 621 (2016).
36. Kravets, V. *et al.* Singular phase nano-optics in plasmonic metamaterials for label-free single-molecule detection. *Nature Materials* **12**, 304 (2013).
37. Kravets, V., Schedin, F., Kabashin, A. & Grigorenko, A. Sensitivity of collective plasmon modes of gold nanoresonators to local environment. *Optics Letters* **35**, 956–958 (2010).
38. Thackray, B. D. *et al.* Narrow collective plasmon resonances in nanostructure arrays observed at normal light incidence for simplified sensing in asymmetric air and water environments. *ACS Photonics* **1**, 1116–1126 (2014).
39. Danilov, A. *et al.* Ultra-narrow surface lattice resonances in plasmonic metamaterial arrays for biosensing applications. *Biosensors and Bioelectronics* **104**, 102–112 (2018).
40. Svedendahl, M., Chen, S., Dmitriev, A. & Kall, M. Refractometric sensing using propagating versus localized surface plasmons: a direct comparison. *Nano Letters* **9**, 4428–4433 (2009).
41. Lin, V. K. *et al.* Dual wavelength sensing based on interacting gold nanodisk trimers. *Nanotechnology* **21**, 305501 (2010).
42. Zhan, Y., Lei, D. Y., Li, X. & Maier, S. A. Plasmonic fano resonances in nanohole quadrimers for ultra-sensitive refractive index sensing. *Nanoscale* **6**, 4705–4715 (2014).
43. Lassiter, J. B. *et al.* Fano resonances in plasmonic nanoclusters: geometrical and chemical tunability. *Nano Letters* **10**, 3184–3189 (2010).
44. Wang, N., Zeisberger, M., Hübner, U. & Schmidt, M. A. Nanotrimer enhanced optical fiber tips implemented by electron beam lithography. *Optical Materials Express* **8**, 2246–2255 (2018).

Acknowledgements

This work is partially funded by Thuringian State via the projects 2015FGI0011, and 2015-0021 partially supported by the European Regional Development Fund (ERDF). N. W. acknowledges funding by China Scholarship Council via contract number 201509110107. We acknowledge financial support for publication from Thuringer Universitäts- und Landesbibliothek Jena (ThULB) and Friedrich-Schiller-University (FSU).

Author Contributions

N.W. and M.A.S. conceived the idea. N.W. conducted the experimental measurements. N.W. and M.Z. performed the numerical simulations. N.W., M.Z., V.G. and M.A.S. analyzed the data and discussed the results. U.H. fabricated the trimer sample. M.A.S. supervised the research. The manuscript was written by N.W., M.Z. and M.A.S. through contributions of all authors. All authors have given approval to the final version of the manuscript.

Additional Information

Supplementary information accompanies this paper at <https://doi.org/10.1038/s41598-019-39779-x>.

Competing Interests: The authors declare no competing interests.

Publisher's note: Springer Nature remains neutral with regard to jurisdictional claims in published maps and institutional affiliations.



Open Access This article is licensed under a Creative Commons Attribution 4.0 International License, which permits use, sharing, adaptation, distribution and reproduction in any medium or format, as long as you give appropriate credit to the original author(s) and the source, provide a link to the Creative Commons license, and indicate if changes were made. The images or other third party material in this article are included in the article's Creative Commons license, unless indicated otherwise in a credit line to the material. If material is not included in the article's Creative Commons license and your intended use is not permitted by statutory regulation or exceeds the permitted use, you will need to obtain permission directly from the copyright holder. To view a copy of this license, visit <http://creativecommons.org/licenses/by/4.0/>.

© The Author(s) 2019